RATE-CONTROLLING TRITIUM TRANSPORT MECHANISMS IN SOLID BREEDERS*

A.R. Raffray, Z.R. Gorbis, and M.A. Abdou
University of California, Los Angeles

I. ABSTRACT

Several transport mechanisms are involved in tritium transport in solid breeders—diffusion in the grain, diffusion along grain boundary, bulk adsorption on the grain boundary/pore interface, desorption to the pores, diffusion along interconnected porosities and convection by the purge flow. It is generally thought that two of the most rate controlling mechanisms are diffusion in the grain and desorption at the grain boundary/pore interface. However, depending on the breeder microstructure, diffusion through the pore can also significantly affect the overall tritium transport process. These three mechanisms are considered here, and the key parameters affecting the tritium transport rate by each mechanism are characterized. Grain diffusion and desorption are first compared, and multi-parameter plots showing regions of diffusion and desorption controls are derived for cases of purge flow with and without hydrogen addition. Grain diffusion is then compared to pore diffusion and the effect of the solid breeder microstructure on the pore diffusion coefficient is discussed. Finally, the resulting equations and plots are applied to experimental data from the LISA1 and TRIO experiments to evaluate the rate-controlling mechanisms.

II. COMPARING GRAIN DIFFUSION TO DESORPTION

Characterization of the grain diffusion rate is straightforward but the complexity arises when characterizing the desorption rate. In a previous work[1], Bertone showed an interesting comparison of the diffusion rate to the desorption rate but in order to obtain his final graph, he had to make a number of assumptions and simplifications, such as: (1) desorption was assumed to be of the first order, whereas at the temperature of operation of solid breeder, chemisorption with dissociation and hence desorption with recombination will probably occur (for e.g., [2]) leading to second order desorption (i.e., proportional to the square of the coverage); the coverage at the grain boundary/pore interface was represented by the local diffusive inventory at the grain edge; and (3) values for the diffusion and desorption activation energies were specified (81.7 kJ/mol and 119 kJ/mol, respectively).

Thus, his graph gives a good indication of the different regions (diffusion control, transition and desorption control) but cannot be used as a more general plot to determine the controlling process for a wide range of conditions.

Comparison of the characteristic times of the two processes to determine the rate controlling step does not seem very useful since at steady state, the coverage will be such that the time for a given quantity of tritium to desorb is equal to the time for the same quantity to diffuse. Of greater interest are the respective inventories at steady state (i.e., the diffusive inventory in a solid breeder grain and the corresponding coverage at the grain boundary/pore interface). It seems reasonable to assume that the larger inventory will be associated with the rate-controlling mechanism and the larger the relative inventory the more rate-controlling the mechanism. The inventory equations derived below are discussed in more details in Ref. [3].

II.1 Diffusive Inventory in Grain

The bulk inventory, I_g, in one solid breeder grain is given by:

$$I_g = I_{go} + I_{g(ads)} \tag{1}$$

$$I_{go} = \frac{r_g^2\, G\, V_g}{15 D_g} \tag{2}$$

$$D_g = D_{go} \exp(-E_{dif}/R_o T) \tag{3}$$

where I_{go} is the inventory assuming zero concentration at the grain boundary and $I_{g(ads)}$ is the inventory due to finite concentration at the grain boundary required for adsorption from the bulk at the grain boundary/pore interface and determined by the coverage there. The other parameters are defined in the Nomenclature Section.

Although $I_{g(ads)}$ is part of the inventory in the bulk, it is controlled by the coverage, and hence, should effectively be considered as a part of the desorption inventory when comparing the diffusive and desorption inventories. Its calculation, though, involves several more parameters, such as the activation energy for adsorption from the bulk, and would make the overall calculations even more complex. It seems reasonable to set $I_{g(ads)} = 0$ and to use ($I_g = I_{go}$) as a measure of the diffusive inventory. Setting $I_{g(ads)}=0$ would result in a lower bound estimate for the desorption inventory (effectively equal to the coverage) and, hence, in a lower bound for the transition region between desorption-control and diffusive-control when comparing desorption to grain diffusion. Arbitrarily, an upper bound for the transition region is then set as 10 times the ratio of diffusive to desorption inventories.

The time for ($I_g = I_{go}$) to diffuse, t_{dif}, is given by:

$$t_{dif} = r_g^2/15 D_g \tag{4}$$

The tritium coverage, $\Delta\theta_{T(dif)}$, equivalent to the diffusive inventory in a grain is:

$$\Delta\theta_{T(dif)} = \frac{2\times10^3\, I_g\, N_o}{n_s\, S_{BET}\, M\, \rho_{SB}\, V_g} \tag{5}$$

II.2 Desorption Inventory (Coverage)

The rate of desorption from the surface for activated desorption with recombination is given by :[4]

$$\frac{d\theta_T}{dt} = \frac{-R_o T}{N_o h}\, \theta_T^2 \exp(-E_{des}/R_o T) \tag{6}$$

* This work was performed under US Department of Energy contract # DE-FG03-86ER52123

For a small change in tritium coverage, $-\Delta\theta_T$ (small enough that E_{des} can be assumed constant), Eq. (6) can be written as:

$$(\Delta t)_{des} = \frac{\Delta\theta_T}{\theta_T^2} \frac{N_o h}{R_o T} \exp(E_{des}/R_o T) \quad (7)$$

The time, t_{des}, for an amount of tritium equivalent to the diffusive inventory to desorb can be obtained by substituting for $\Delta\theta_{T(dif)}$ from Eq. (5) in Eq. (7):

$$t_{des} = \frac{2\times10^3 I_g N_o}{n_s S_{BET} M \rho_{SB} V_g} \frac{1}{\theta_T^2} \frac{N_o h}{R_o T} \exp(E_{des}/R_o T) \quad (8)$$

At steady state, the time for a given amount, I_g, of tritium to diffuse is equal to the time for the same amount to desorb. Therefore, equating Eqs. (4) and (8), substituting for I_g from Eq. (2) and solving for θ_T yields:

$$\theta_T = \left(\frac{2\times10^3 G N_o}{n_s S_{BET} M \rho_{SB}}\right)^{1/2} \left(\frac{N_o h}{R_o T}\right)^{1/2} \exp(E_{des}/2R_o T) \quad (9)$$

II.3 Diffusive to Desorption Inventories

(i) No hydrogen in the purge

Comparing the diffusive inventory (represented by $\Delta\theta_{T(dif)}$ in Eq. (5)) to the adsorption inventory (represented by θ_T in Eq. (9)) and substituting for I_g from Eq. (2) gives:

$$\frac{\Delta\theta_{T(dif)}}{\theta_T} = \left(\frac{\Delta\theta_{T(dif)}}{D_{go}}\right)^{1/2} r_g \left(\frac{T}{A_1}\right)^{1/2} \exp(-\Delta E/2R_o T) \quad (10)$$

where $\Delta\theta_{T(dif)}$ is described in Eq. (5) and the other parameters are described in the Nomenclature Section.

(ii) Hydrogen in the purge

If there is hydrogen in the purge with a corresponding hydrogen coverage, θ_H, the total coverage, θ_{TOT}, becomes:

$$\theta_{TOT} = \theta_T + \theta_H \quad (11)$$

Then θ_T^2 in Eq. (6) should be replaced by $\theta_T[\theta_T + \theta_H]$ which can be approximated by $\theta_T\theta_H$ for $\theta_H >> \theta_T$.

Eqs. (9) and (10) then become:

$$\theta_T = \frac{2\times10_3 G N_o}{n_s S_{BET} M \rho_{SB}} \frac{N_o h}{R_o T} \frac{1}{\theta_H} \exp(E_{des}/R_o T) \quad (12)$$

$$\frac{\Delta\theta_{T(dif)}}{\theta_T} = \frac{\theta_H}{D_{go}} r_g^2 \frac{T}{A_1} \exp(-\Delta E/R_o T) \quad (13)$$

θ_H then needs to be determined independently based on the hydrogen partial pressure, P_{H_2}, in the purge :[4]

$$\left(\frac{1}{\theta_H} - 1\right)^2 = n_s \left(\frac{R_o T}{N_o}\right)^{3/2} \frac{\sqrt{2\pi m_{H_2}}}{C_c P_{H_2} h} \exp(-q_{ads}/R_o T) \quad (14)$$

where the parameters are described in the Nomenclature Section. Note that for large θ_H (tending to 1), desorption is effectively proportional to θ_T (i.e., first order).

II.4 Graphical Representation of Results

Both Eqs. (10) and (13) are quite complex and it seems difficult to come up with a simple graph to determine the rate-controlling mechanism. An attempt has been made to plot both equations for different values of ΔE's, as shown on Figs. 1 and 2. Figure 1 shows a plot of $(\Delta\theta_{T(dif)}/\theta_T)$ as a function of $(\Delta\theta_{T(dif)}/D_{go})^{1/2} r_g$, ΔE and temperature, applicable to the case where there is no hydrogen in the purge. Figure 2 shows a plot of $(\Delta\theta_{T(dif)}/\theta_T)$ as a function of $(\theta_H/D_{go}) r_g^2$, ΔE and temperature, applicable to the case where there is hydrogen in the purge which swamps the tritium so that the hydrogen coverage is much larger than the tritium coverage ($\theta_H >> \theta_T$).

Arbitrarily, as explained earlier, the transition region (shaded on the plot) for each ΔE has been set to correspond to the region between $(\Delta\theta_{T(dif)}/\theta_T)$ based on setting $I_{g(ads)} = 0$ and $10(\Delta\theta_{T(dif)}/\theta_T)$. The solid lines thus represent 10 $(\Delta\theta_{T(dif)}/\theta_T)$ and the dashed lines $(\Delta\theta_{T(dif)}/\theta_T)$. Above the transition region, grain diffusion is the rate-controlling mechanism; and below the transition region, desorption is the rate-controlling mechanism.

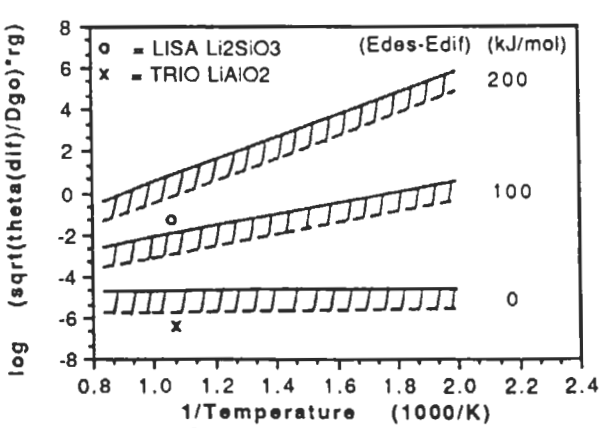

Figure 1: Regions of grain diffusion control and desorption control as a function of temperature and of a comparison parameter for different differential activation energies for cases with no hydrogen in the purge. (Shaded area represents transition region above which grain diffusion is rate-controlling, and below which desorption is rate-controlling).

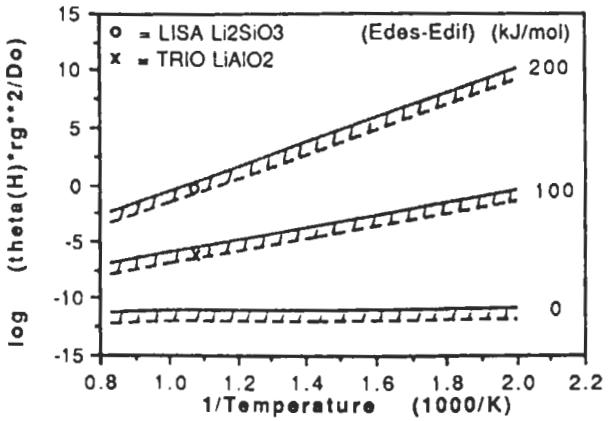

Figure 2: Regions of grain diffusion control and desorption control as a function of temperature and of a comparison parameter for different differential activation energies for cases with hydrogen added to the purge. (Shaded area represents transition region above which grain diffusion is rate-controlling, and below which desorption is rate-controlling).

Thus, in order to determine the rate-controlling mechanism, the following parameters need to be known:

For cases with no hydrogen in the purge: r_g, G, V_g , D_{go}, E_{dif}, n_s S_{BET}, ρ_{SB}, ΔE, T.

For cases with hydrogen swamping in the purge: n_s, T, P_{H2}, C_c, q_{ads}, D_{go}, ΔE, r_g.

These are long lists of parameters, which could be simplified to a first order approximation if some of them are assumed to be roughly equal for different breeders (e.g., C_c, n_s, and ρ_{SB}). Still, the mechanisms are such that several parameters need to be known to determine the rate-controlling mechanism. Note that in both cases, the vertical axis dependency is on r_g^2, not on r_g, since in Fig. 1, $(\Delta\theta_{T(dif)})^{1/2}$ is proportional to r_g.

III. Comparing Pore Diffusion to Grain Diffusion

The comparison of these two diffusion mechanisms is done based on their respective tritium inventories at steady-state for a bulk tritium generation rate per unit volume, G. The grain diffusive inventory in this case is given by Eq. (2). The pore diffusive inventory normalized to one grain can be derived starting from the steady-state 1-D diffusion equation. Assuming a system of open interconnected porosity of average radius r_{ip}, and of effective length, L_e, and assuming a constant effective tritium pore diffusion coefficient, D_{Peff}.

$$D_{Peff}\frac{d^2C_p}{dz^2} = -\frac{G\,V_g}{V_{ip}} \tag{15}$$

where V_{ip} is the volume of a system of open interconnected porosity. Eq. (15) can be integrated twice to obtain an expression for the local tritium pore concentration per unit volume assuming boundary conditions of zero concentration gradient at z = 0 and zero concentration at z = L_e, where the tritium is convected by the purge flow.

Integration of the concentration over L_e results in the following expression for the pore tritium inventory, I_p:

$$I_p = \frac{G\,V_g\,L_e^2}{3D_{Peff}} \tag{16}$$

L_e, the effective pore length can be calculated from the physical length, L, using a tortuosity factor based on the open porosity, ε:[5]

$$L_e = \frac{L}{\sqrt{\varepsilon}} \tag{17}$$

Comparison of I_p from Eq. (16) to ($I_g = I_{go}$) from Eq. (2) gives:

$$\frac{I_p}{I_g} = \frac{5L^2\,D_{go}}{\varepsilon r_g^2\,D_{Peff}}\exp(-E_{dif}/R_oT) \tag{18}$$

The pore diffusion coefficient depends on the diffusion regime and is discussed in the next section.

III.1 Pore Diffusion Coefficient

According to Youngquist[6], three different diffusion regimes are possible, namely, (1) ordinary diffusion in which molecular collisions dominate the diffusion process, (2) Knudsen diffusion in which collisions of the diffusing molecules with the porous solid dominate the diffusion process, and (3) a transition region between the above two diffusion regimes. Which regime applies depends on the Knudsen number, K_n, defined as the ratio of the mean-free-path of the diffusion species, λ, to the characteristic pore radius, r_{ip}. A value of $K_n < 0.10$ results in ordinary diffusion, while $K_n > 10.0$ results in Knudsen diffusion, and $0.10 < K_n < 10.0$ results in transition region diffusion.

To define the applicable regime, the mean-free-path, λ, and the representative channel radius, r_{ip}, are required. They can be estimated from the following expressions:

$$r_{ip} = \frac{2\,\varepsilon}{\rho_{SB}\,(1-\varepsilon)\,S_{BET}} \tag{19}$$

$$\lambda = \frac{k_BT}{\sqrt{2}\pi\sigma^2P} \tag{20}$$

where k_B is Boltzmann's constant, σ is the constant in the Lennard-Jones potential energy function (in meters) and P is the gas pressure in Pascals.

For flow of binary mixtures in a single capillary the Knudsen diffusion coefficient, D_k, is given by:

$$D_k = \frac{2}{3}r_{ip}\sqrt{\frac{8R_oT}{\pi M}} \tag{21}$$

For ordinary diffusion at low pressure, the Chapman-Enskog formula for the diffusion coefficient, D_o, can be employed:[7]

$$D_o = 1.8583 \times 10^{-7}\frac{T^{3/2}\sqrt{1/M+1/M_{He}}}{P\sigma\Omega} \tag{22}$$

where P is in atmospheres of pressure, σ in Å, and Ω is the collision integral.

Finally, for the transition region, the expression for the transition coefficient, D_T derived by Youngquist[6] is proposed under the assumption of very low mole fraction of the diffusing species.

$$D_T = 1/\left(\frac{1}{D_o} + \frac{1}{D_k}\right) \quad (23)$$

III.2 Microstructure Effect on Pore Diffusion Coefficient

The pore diffusion coefficient, D_p, can be calculated from Eqs. (21), (22) or (23) depending on the diffusion regime. However, the final effective pore diffusion coefficient, $D_{P_{eff}}$, can differ substantially from D_p depending on the breeder microstructure, as discussed in Ref. [8]. For example, a series of expansions and constrictions associated with different pore diffusion can significantly affect $D_{P_{eff}}$. Michaels[9] considered two cylindrical pores, one of radius r_{p1} and length l_{p1} and the other of radius r_{p2} and length l_{p2}, which are connected in series. The pore system may be considered as composed of any number of these characteristic units in series. Since the diffusional resistance offered by any one of these units is the same as any other, it is possible by characterizing the unit to characterize thereby the entire pore. By assuming the same flux through each cylindrical pore and through an equivalent uniform pore of average volume per unit length similar to that of the unit, Michaels derived the following equation:

$$\frac{D_{p_{ave}}}{D_{p_{eff}}} = 1 + \frac{L_p}{(L_p+1)^2}\left(\frac{R_p^2 - 1}{R_p}\right)^2 \quad (24)$$

where $D_{p_{ave}}$ is the average pore diffusion coefficient through each cylindrical pore, $D_{p_{eff}}$ is the effective pore diffusion coefficient due to constriction and expansion effects, $L_p = l_{p1}/l_{p2}$, and $R_p = r_{p1}/r_{p2}$.

It is important to note that the above reduction in the pore diffusion coefficient is solely due to a series of constrictions and expansions in the pore diffusive path and was obtained using a constant $D_{p_{ave}}$ independent of the local pore sizes. This is the case if ordinary diffusion prevails. However, if diffusion occurs even partially in the Knudsen or transition regimes, $D_{p_{ave}}$ should then be estimated as an average pore diffusion coefficient by taking into account the pore size distribution as described in Section IV.2. The value of this average pore diffusion coefficient can be quite different from D_p, the value obtained from the average pore radius.

III.3 Graphical Representation of Results

As discussed in the previous section, the diffusion regime depends on r_{ip} and λ. Figure 3 shows the diffusion regime as a function of the pore radius and temperature for tritium diffusion in helium based on the Knudsen number and Eq. (20). Typically, depending on the temperature, for pore radii of the order of 1 micron or more ordinary diffusion prevails while for pore radii of the order of 0.01 micron or less, Knudsen diffusion prevails. The transition regime occurs in between these pore radii. The pore diffusion coefficient D_p calculated from Eqs. (21), (22) or (23) is plotted in Fig. 4 as a function of temperature and of the average pore radius. Finally, to graphically illustrate the pore to grain tritium inventory comparison, Eq. (18) is plotted in Fig. 5 in terms of a pore to grain comparison parameter K_{pg}, and of temperature for different values of the grain diffusion activation energy. K_{pg} is defined as follows:

$$K_{pg} = \frac{5\, L^2\, D_{go}}{\varepsilon\, r_g^2\, D_{p_{eff}}} \quad (25)$$

From Fig. 5, the region above each line for the given parameters corresponds to pore diffusion being more rate-controlling than grain diffusion and vice versa for the region below each line.

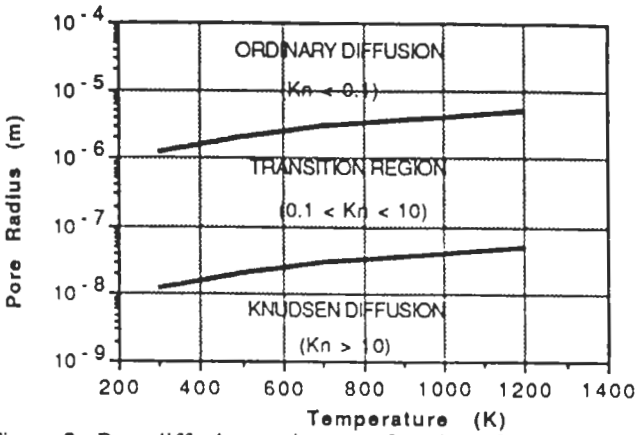

Figure 3: Pore diffusion regime as a function of pore radius and temperature for a pressure of 1 atm.

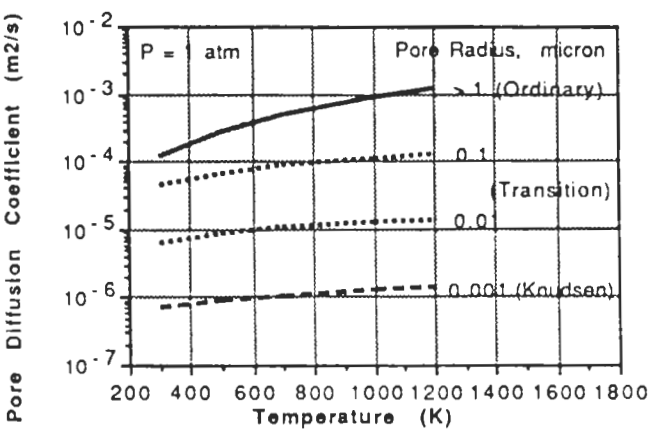

Figure 4: Pore diffusion coefficient as a function of temperature for different pore radius (the diffusion regime is shown in parentheses for each case).

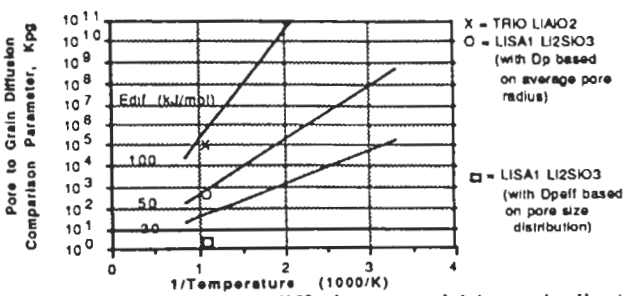

Figure 5: Regions of pore diffusion control (above the line) and grain diffusion control (below the line) as a function of a comparison parameter and temperature for different grain diffusion activation energies.

Thus, parameters of importance in comparing pore diffusion to grain diffusion are: L, D_{go}, E_{dif}, T, r_g^2, ϵ, ρ_{SB}, S_{BET}, P and pore size distribution and magnitude. This list could be shortened by assuming that ρ_{SB}, for example, is of the same order for different breeders and by normalizing the length, L, to 1 cm and P to 1 atm but still leaves 6 determinant parameters in addition to the pore size distribution and magnitude which must be characterized in order to determine the diffusive rate-controlling mechanism.

IV. APPLYING THE RESULTS TO TRIO AND LISA EXPERIMENTAL DATA

IV.1 Grain Diffusion vs. Desorption

The grain diffusion/desorption comparison parameters of interest can be calculated from typical experimental conditions for the TRIO[10] $LiAlO_2$ sample and the LISA1[11] Li_2SiO_3 sample based on the data listed in Table 1. The results are summarized in Table 2 and also shown on Figures 1 and 2.

Table 1: Parameters Used for TRIO and LISA Calculations

	TRIO[10]	LISA1[11]
r_g (μm)	0.1	39.5
G (kg/m^3-s)	3.98×10^{-8}	4.9×10^{-8}
D_{go} (m^2/s)	2×10^{-9} [12]	7.9×10^{-10} [12]
E_{dif} (J/mol)	9×10^4 [12]	7.8×10^4 [12]
T (K)	923	923
n_s (sites/m^2)	10^{19}	10^{19}
S_{BET} (m^2/kg)	450	770 (estimated from [13])
ρ_{SB} (TD, kg/m^3)	2613	2520
ϵ (open)	0.35	0.12
L(cm)	0.5	0.36

As shown in Fig. 1, for the case with no H_2 in the purge, if (E_{des} - E_{dif}) is about 140 kJ/mol or less, diffusion was the rate-controlling mechanism for the LISA experiment. If (E_{des} - E_{dif}) is about 180 kJ/mol or more, then desorption was the rate-controlling mechanism. For TRIO, if E_{des} is greater than E_{dif}, desorption was the rate-controlling mechanism. Ref. [2] gives values for heat of adsorption as a function of coverage for the adsorption of water vapor on $LiAlO_2$. These data were used in the absence of similar data for the $LiAlO_2$-H_2 system. The activation energy for desorption is equal to the sum of the heat of adsorption and the activation energy for adsorption which tends to be small. Thus, the heat of adsorption values can be viewed as lower bounds for the activation energy for desorption. Based on Ref. [2], for these types of low coverage (of the order of 0.001), the activation energy for desorption then is at least of the order of 360 kJ/mol for $LiAlO_2$. Thus ΔE is at least about 260 kJ/mol for $LiAlO_2$, which indicates that the TRIO runs with no H_2 in the purge were desorption-controlled. For LISA, the indications are not so clear, since for desorption rate control, E_{des} must be about 260 kJ/mol or more. If E_{des} for Li_2SiO_3 is assumed to be similar to that for $LiAlO_2$, then for LISA also, desorption was the rate-controlling step for cases with no H_2 in the purge.

Table 2: Grain Diffusion/Desorption Comparison Parameters for TRIO $LiAlO_2$ and LISA1 Li_2SiO_3 Samples for Cases with and without Hydrogen in the Purge.

	TRIO	LISA1
No Hydrogen in the purge		
D_g (m^2/s)	1.61×10^{-14}	3.04×10^{-14}
$(I_g/V_g)$from Eq.(2) (kg/m^3)	1.65×10^{-9}	1.68×10^{-4}
$\Delta\theta_{T(dif)}$ from Eq. (5)	2.83×10^{-8}	1.73×10^{-3}
$\log((\Delta\theta_{T(dif)}/D_{go})^{1/2}r_g)$	-6.43	-1.233
0.1% H_2 in the purge		
P_{H_2} (Pa)	340[10]	200(assumed)
q_{ads} (kJ/mol) [2]	9×10^4	9×10^4
θ_H from Eq. (18) and q_{ads}	0.079	0.054
$\log(\theta_H r_g^2/D_{go})$	-6.40	-0.973

From Fig. 2, for the LISA case with 0.1% H_2 in the purge, ΔE must be lower than about 190 kJ/mol for diffusion to be rate-controlling and higher than about 210 kJ/mol for desorption to be rate-controlling. For TRIO, ΔE must be lower than about 90 kJ/mol for diffusion to be rate-controlling, and higher than about 110 kJ/mol for desorption to be rate-controlling. In both cases, with H_2 in the purge the control shifts toward diffusion because, with the high H_2 coverage, desorption is faster. For the type of H_2 coverage calculated (0.05-0.1), E_{des} is higher than about 100 - 150 kJ/mol from Ref. [2]. If a value of 150 kJ/mol is assumed, ΔE is about 70 kJ/mol for Li_2SiO_3 and 60 kJ/mol for $LiAlO_2$. This indicates that the presence of 0.1% H_2 has caused diffusion to be the rate-controlling mechanism for both LISA and TRIO, based on the assumed property data.

IV.2 Pore Diffusion vs. Grain Diffusion

From the data in Table 1, the parameters in Table 3 can be estimated for the TRIO $LiAlO_2$ and Li_2SiO_3 samples.

Table 3: Pore/Grain Diffusion Comparison Parameters for TRIO $LiAlO_2$ and LISA1 Li_2SiO_3 Samples.

	TRIO	LISA1
$(S_{BET}\,\rho_{SB})$ (m^2/m^3)	1.17×10^6	1.94×10^6
r_{ip} from Eq.(19) (micron)	5	0.13
D_p from Fig.4 (m^2/s)	7.5×10^{-4}	1.3×10^{-4}
K_{pg} from Eq.(25)(based on D_p)	9.5×10^4	2.1

From Fig. 5, for 1000/T = 1.08, the TRIO point falls very close to the transition between pore diffusion and grain diffusion control for E_{dif} = 90 kJ/mol. If the property data used are correct this illustrates the importance of pore diffusion as a transport mechanism. In addition, in the absence of data, the effect of the pore microstructure was not accounted for. It is likely that any significant distribution of pore sizes would make pore diffusion slower and thus, more rate controlling.

For the LISA1 sample, from Fig. 5, grain diffusion is significantly slower than pore diffusion even if E_{dif} is much lower than reported in Ref. [12]. However, this particular Li_2SiO_3 sample is a notable exception in that its pore size distribution has been characterized experimentally[13], as shown in Fig. 6. The distribution

covers a wide range of pore sizes and can be considered bimodal with distribution peaks corresponding to mean pore diameters of about 35 and 1500 nm.

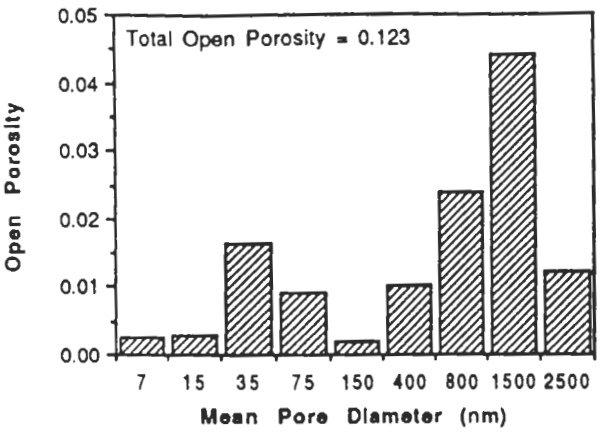

Figure 6 Open porosity associated with different mean pore diameters for the LISA1 Li_2SiO_3 sample (from Ref. [13].

Using $R_p = 1500/35$ and assuming, in the absence of specific data, that $L_p = R_p$, Eq. (24) yields:

$$\frac{D_{p_{eff}}}{D_{p_{ave}}} = 0.023 \tag{26}$$

This reduction in the pore diffusion coefficient is solely due to a series of constrictions and expansions. In addition, if diffusion occurs in the Knudsen or transition regimes, $D_{p_{ave}}$ should be estimated based on the pore size distribution.

From Fig. 6, the local porosity, ε_{p_j}, and the associated pore radius, r_{p_j}, can be combined to obtain an effective characteristic length, $(\varepsilon_{p_j}/r_{p_j}^2)$, for diffusion through each pore size, j. The diffusion coefficient, D_{p_j}, associated with each pore size can be calculated based on the local diffusion regime. The time constant for diffusion through each pore size is then given by $(\varepsilon_{p_j}^2/r_{p_j}^4 D_{p_j})$. The average diffusion coefficient, $D_{p_{ave}}$, can then be estimated by equating the summation of time constants for diffusion through each pore size to the overall time constant for diffusion.

$$D_{p_{ave}} = \frac{(\Sigma_{j-1}^{n}(\varepsilon_{p_j}/r_{p_j}^2))^2}{\Sigma_{j-1}^{n}(\varepsilon_{p_j}^2/r_{p_j}^4 D_{p_j})} \tag{27}$$

Doing this calculation for the LISA1 Li_2SiO_3 sample yields:

$$D_{p_{ave}}/D_p = 0.14 \tag{28}$$

Thus combining the effects of changes in the local pore diffusion coefficient with those of constrictions and expansions in the interconnected pore system (Eqs.. (46) and (48) results in:

$$D_{p_{eff}}/D_p = 0.0033 \tag{29}$$

This value gives a good indication of what the effective pore diffusion coefficient should be but still carries some uncertainty. For example, the effect of constrictions and expansions was estimated assuming only two pore sizes for calculation simplicity. Accounting for the numerous pore sizes shown in Fig. 6 might yield a different answer.

Increasing K_{pg} of Table 3 by the ratio of Eq. (29) gives a new value of 636. From Fig. 5, pore diffusion becomes substantially more important and would be rate controlling for an E_{dif} of about 50 kJ/mol or less. This is still lower than the value of 78 kJ/mol obtained for Ref. [12]. However, it must be noted that the grain diameter is quite large for this Li_2SiO_3 sample which reduces appreciably the rate of tritium diffusion in the grain.

This example illustrates to what extent pore diffusion can be slowed down when accounting for the pore microstructure and indicates the importance of characterizing the magnitude and distribution of pore sizes for solid breeders. For the $LiAlO_2$ sample of TRIO for example, even a small decrease in pore diffusion would cause it to be the diffusive rate controlling mechanism. This is of even more importance for cases where hydrogen is added to the purge since hydrogen diffusion through the pores would also be affected and since the discussion in Section IV.1 has shown that grain diffusion tends to be slower than desorption for these cases. It follows that if pore diffusion is slower than grain diffusion, it would be the rate controlling mechanism (when compared to both grain diffusion and desorption).

V. SUMMARY

Comparisons of grain diffusion to desorption and of pore diffusion to grain diffusion were done in order to assess their relative importance as rate-controlling mechanisms for tritium transport in solid breeders. Because of the complexity involved in deriving expressions for such comparisons, some simplifications were introduced, in particular for boundary conditions. Overall, though, the comparison results are believed to give a proper assessment of the relative importance of these tritium transport mechanisms.

Several parameters need to be known to evaluate both comparisons, in particular the grain diffusion coefficient pre-exponential and activation energy, the desorption activation energy, and the breeder microstructure (namely, the given radius, specific surface area, open porosity and pore size distribution). These need to be characterized in order to properly evaluate the tritium transport process. A summary of each comparison follows:

V.1 Grain Diffusion vs. Desorption

The ratio of diffusive to desorption inventories was used for the comparison for both cases with and without H_2 in the purge. The results were plotted on two general graphs in terms of temperature, differential activation energy and a comparison parameter for each case. Calculations for TRIO and LISA1 comparing grain diffusion to desorption from the assumed property data indicate that for both cases, desorption was the rate-controlling step when there was no H_2 in the purge and diffusion was the rate-controlling step when there was 0.1% H_2 in the purge.

V.2 Pore Diffusion vs. Grain Diffusion

The ratio of pore to grain diffusive inventory normalized to the tritium generation rate in one grain was used for the comparison, and the final expression was plotted in terms of the temperature, grain diffusion activation energy and a comparison parameter, K_{pg}. K_{pg} is inversely proportional to the effective pore diffusion coefficient which is evaluated according to the diffusion regime.

The breeder microstructure, in particular a wide pore size distribution, can significantly affect pore diffusion. The average pore diffusion coefficient calculated from the local pore size distribution can be substantially lower than that based on the average pore radius. In addition, a series of

constrictions and expansions can be shown to further reduce the pore diffusion coefficient. Both these effects need to be incorporated when calculating the effective pore diffusion coefficient.

Calculations for the TRIO $LiAlO_2$ sample indicate that it operated close to the transition between pore diffusion and grain diffusion rate control. However, in the absence of detailed microstructure characterization, the effective pore diffusion coefficient was based on the average pore radius only. Any reduction in the pore diffusion coefficient due to a significant pore size distribution could result in pore diffusion being rate controlling. For the Li_2SiO_3 sample in LISA1 grain diffusion seems to have been rate-controlling due to the large grain diameter. However, it must be noted that proper accountability of the pore size distribution which was characterized in this case reduces the pore diffusion coefficient by a factor of 300.

Pore diffusion can thus be rate-controlling depending on the breeder microstructure, in particular for cases where hydrogen is added in the purge and where grain diffusion seems to be slower than desorption. In addition, the hydrogen diffusion through the pores and the resulting adsorption/desorption processes are also affected by the pore diffusion coefficient.

NOMENCLATURE

A_1 = $\frac{15\,N_o h}{R_o}$

C_c = condensation coefficient ≈ 0.4

C_p = tritium concentration in the pore (kg/m^3)

D_g = grain diffusion coefficient (m^2/s)

D_{g_o} = grain diffusion coefficient pre-exponential (m^2/s)

D_k = Knudsen pore diffusion

D_o = ordinary pore diffusion coefficient (m^2/s)

D_p = pore diffusion coefficient based on average pore radius, r_{ip}, (m^2/s)

$D_{p_{ave}}$ = average pore diffusion coefficient based on local pore size distribution (m^2/s)

$D_{p_{eff}}$ = effective pore diffusion coefficient (m^2/s)

D_T = transition pore diffusion coefficient (m^2s)

E_{des} = activation energy for desorption (J/mol)

E_{dif} = activation energy for grain diffusion (J/mol)

ΔE = $E_{des} - E_{dif}$

G = bulk tritium volumetric generation rate (kg/m^3-s)

h = Planck's constant = 6.63×10^{-34} J-s

I_g = tritium inventory in one solid breeder grain (kg)

$I_{g(ads)}$ = tritium inventory in one solid breeder grain due to finite concentration at grain boundary (kg)

I_{g_o} = tritium inventory in one solid breeder grain assuming zero concentration at the grain boundary (kg)

I_p = pore tritium inventory normalized to one grain (kg)

k_B = Boltzmann's constant = 1.38×10^{-23} J/K

Kn = Knudsen number

K_{pg} = pore to grain comparison parameter (see Eq. (29))

l_p = local pore length (m)

L = physical length of pore diffusion path (m)

L_e = effective length of pore diffusion path = $L/\sqrt{\varepsilon}$ (m)

L_p = l_{p1}/l_{p2}

m_{H_2} = mass of one hydrogen molecule = 3.32×10^{-27} kg

M = molecular weight of tritium = 6 kg/kmol

M_{He} = molecular weight of helium = 4 kg/kmol

n_s = number of sites per unit surface area ≈ 10^{19} sites/m^2

N_o = Avogadro's number = 6.02×10^{23} molecules/mol

P = total pressure

P_{H_2} = hydrogen partial pressure (Pa)

q_{ads} = heat of adsorption (J/mol)

r_{ip} = average radius of open interconnected porosity system (m)

r_g = grain radius (m)

r_p = local pore radius (m)

R_o = universal gas constant = 8.3143 J/mol-K

R_p = r_{p1}/r_{p2}

S_{BET} = specific surface area (m^2/kg)

t = time (s)

t_{dif} = time needed for I_g to diffuse through the grain (s)

t_{des} = time needed for I_g to desorb (s)

T = temperature (K)

V_{ip} = volume of open interconnected porosity system (m^3)

V_g = volume of grain (m^3)

z = axial distance along the open interconnected porosity system (m).

ε = solid breeder open porosity

ε_p = local porosity

ρ_{SB} = solid breeder theoretical density (kg/m^3)

θ_H = hydrogen coverage

θ_T = tritium coverage

θ_{TOT} = total coverage = $\theta_H + \theta_T$

$\Delta\theta_{T(dif)}$ = tritium coverage equivalent to the diffusive inventory in one grain

λ = mean free-path of diffusing species

σ = Lennard-Jones potential-energy function = 2.746×10^{-10}m for H_2 in He

Ω = collision integral = $f(k_B/T)$

ACKNOWLEDGEMENT

The authors would like to thank Drs. G. Federici, P. Gierszewski, C. Johnson and J. Kopasz for their valuable input.

REFERENCES

1. P.C. BERTONE, "The Kinetics that Govern the Release of Tritium for Neutron-Irradiated Lithium Oxide," Journal of Nuclear Materials, 151, 281-292 (1988).
2. A. FISCHER and C. JOHNSON, "Measurements of Adsorption in the $LiAlO_2$-H_2O(g) System," Presented at the Eighth Topical Meeting on the Technology of Fusion Energy, Salt Lake City (October 1988).
3. A. R. RAFFRAY, "Comparing Grain Diffusion to Desorption as Rate-Controlling Mechanisms for Tritium Transport in Solid Breeders," UCLA-FNT-39 (March 1990).
4. D.O. HAYWARD and B.M.W. Trapnell, Chemisorption, second edition. Butterworth, London (1964).
5. N. WAKAO and J. M. SMITH, Chem. Eng. Sci., 17, 825 (1962).
6. G.R. YOUNGQUIST, Ind. Eng. Chem., 62-8, 52 (1970).
7. R. B. BIRD, W. E. STEWARD and E. N. LIGHTFOOT, Transport Phenomena, Wiley, New York, London (1960).
8. G. FEDERICI, A. R. RAFFRAY and M. A. ABDOU, "MISTRAL: A Comprehensive Model for Tritium Transport in Lithium-Base Ceramics - Part II: Comparison of Model Predictions with Experimental Results," Journal of Nuclear Materials, 173, 214-228 (1990).
9. A. S. MICHAELS, AICHE J., 270-271 (June 1959).
10. R.G. CLEMMER, et al., "The TRIO Experiment," ANL-84-55, Argonne National Laboratory (September 1984).
11. H. WERLE, et al., "The LISA 1 Experiment: In-Situ Tritium Release Investigations," Journal of Nuclear Materials, 141-143, 321-326 (1986).
12. K. OKUNO, and H. KUDO, "Tritium Diffusivity in Lithium-Base Ceramic Breeders Irradiated with Neutrons," Journal of Nuclear Materials, 8, 355 (1989).
13. H. ELBEL, "Open Pore Structural Analysis of Lithium Bearing Ceramics," Journal of Nuclear Materials, 155-157, 484-488 (1988).